Journal of Green Energy Research and Innovation

Nonlinear Control of Single-Phase Grid-Connected Z-Source Inverters Using MIMO Interconnection and Damping Assignment Passivity-Based Controller

Gholamreza Shahabadi, Siavash Es'haghi, Javad Porhossein

Highlights

- **A novel MIMO IDA-PBC scheme is developed for single-phase grid-connected Z-source inverters, enabling simultaneous regulation of multiple state variables.**
- **The proposed control approach is based on a port-controlled Hamiltonian (PCH) reformulation of the averaged ZSI model, ensuring energy-based system stabilization.**
- **Asymptotic stability and zero steady-state error are analytically guaranteed through Lyapunov-based analysis under the proposed IDA-PBC control.**
- **The control strategy achieves robust performance against parameter variations and ensures accurate tracking of both DC-link voltage and AC grid current references.**

Graphical Abstract

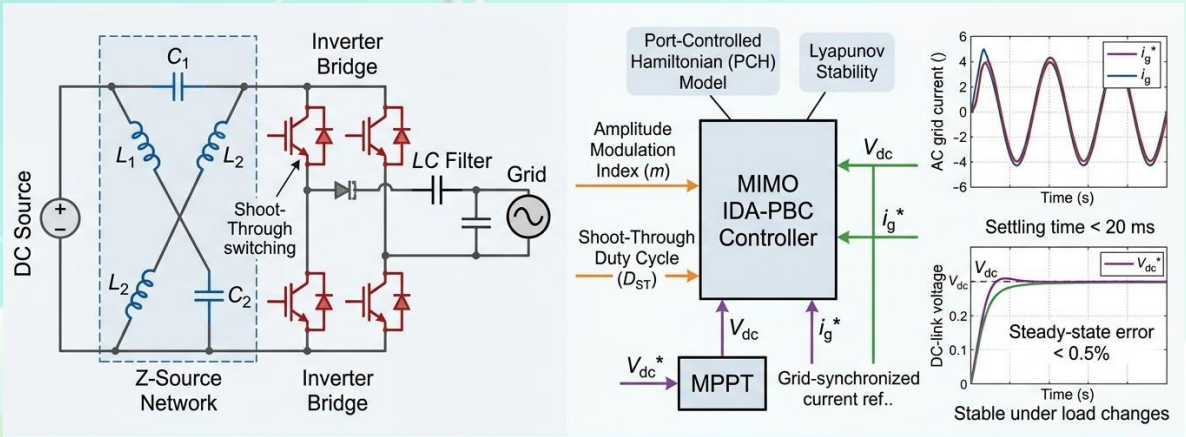

MIMO IDA-PBC enables independent regulation of DC-link voltage and grid current in single-phase Z-source inverters with fast transient response and high stability

Use your device to scan and read the article online

Citation

G. R. Shahabadi, S. Es'haghi, and J. Pourhossein, "Nonlinear Control of Single-Phase Grid-Connected Z-Source Inverters Using MIMO Interconnection and Damping Assignment Passivity-Based Controller," *Journal of Green Energy Research and Innovation*, vol. 3, no. 3, pp. 30-46, 2026.

https://doi.org/10.61882/jgeri.3.3.30

CC BY NC

Journal of Green Energy Research and Innovation 3.3 (2026) 30-46

Online ISSN: 3041-9018

Journal of Green Energy Research and Innovation

Journal Homepage: www.jgeri.araku.ac.ir

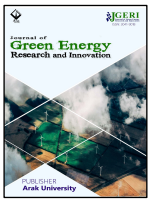

Nonlinear Control of Single-Phase Grid-Connected Z-Source Inverters Using MIMO Interconnection and Damping Assignment Passivity-Based Controller

Gholamreza Shahabadi [1,*], Siavash Es'haghi [2], Javad Porhossein [3]

[1] *Department of Electrical Engineering, National University of Skills (NUS), Tehran, Iran.*

[2] *Department of Electrical engineering, Science and Research Branch, Islamic Azad University, Tehran, Iran.*

[2] *Department of Electrical engineering, Gonabad Branch, Islamic Azad University, Gonabad, Iran.*

A R T I C L E I N F O

Keywords:
Z-Source inverter,
grid-connected inverter,
IDA-PBC,
robust control.

Article History:
Received: 01 July 2025;
Revised: 10 August 2025;
Accepted: 18 August 2025.

Article type:
Research Article

* *Corresponding author*
E-mail address:
Ghr.shahabady@gmail.com (Gh. Shahabadi)

A B S T R A C T

The Z-source inverter (ZSI) represents an effective topology for integrating renewable energy units, as it can inherently perform voltage boosting and bucking within a single conversion stage. For renewable-based distribution systems, maintaining proper grid connection, voltage regulation, and maximum power extraction generally requires a suitable closed-loop control strategy. Classical linear controllers are typically designed around a fixed operating point and therefore struggle to ensure stable performance for nonlinear systems subject to broad operating variations. In this study, a new multi-input multi-output (MIMO) control strategy based on Interconnection and Damping Assignment Passivity-Based Control (IDA-PBC) is introduced for the grid-connected single-phase ZSI. The system's dynamic response is first represented through a state-space averaging model, which is then reformulated within the port-controlled Hamiltonian (PCH) structure. Using this framework, the proposed controller simultaneously regulates key system states, such as the grid-side current and the voltage across the DC-link capacitors, by manipulating the amplitude modulation index and shoot-through duty ratio. Through Lyapunov-based reasoning, the closed-loop stability and asymptotic tracking capability of the controller are formally established. Simulation studies confirm that the proposed method provides fast transient behavior (settling times below 20 ms), nearly zero steady-state error, and retains stable operation under parameter variations and load disturbances. The obtained results highlight improved robustness and superior dynamic behavior compared to conventional linear control techniques.

1. Introduction

In the last decade, grid-integrated DC-AC power conversion systems have attracted a lot of attention. This growing interest is mainly due to the rapid expansion of distributed generation technologies, the increasing penetration of renewable energy sources, and the continuous demand for efficient and reliable power electronic interfaces. Nowadays, these inverters are extensively applied to diverse applications, such as high-voltage direct current (HVDC) transmission systems, renewable energy conversion units, electric vehicles, power quality conditioners, motor drives, and line-interactive uninterruptible power supply (UPS) architectures [1,2]. In addition to these applications, grid-connected inverters play a key role in modern smart grids by enabling bidirectional power flow, voltage regulation, frequency support, and improved power management. Energy generated by renewable sources often has a low voltage level, so it needs to be increased to an acceptable level before being used or injected into the grid [3]. For instance, photovoltaic panels, fuel cells, and battery energy storage systems usually provide variable and relatively low DC voltages, which are not directly suitable for many grid-connected or high-power applications.

In order to address this issue, one approach involves boosting the inverter output voltage using a transformer. Although this method is technically straightforward and widely used in conventional systems, it may not always be the most efficient or compact solution. Another solution is utilizing a power electronic converter interfaced between the DC energy source and the inverter stage. Such a configuration can regulate the DC-link voltage and improve the flexibility of the overall conversion system; however, it generally increases the number of conversion stages and may reduce the total efficiency. Employing transformers significantly raises both the overall expense and the physical size of the system. Moreover, transformers add extra losses, increase system weight, and may negatively affect the dynamic performance of the converter, especially in applications where compactness and high power density are important design objectives. Impedance-source inverter, known as Z-source inverter (ZSI), has been recently exploited as an efficient technique to overcome above-mentioned limitations [4]. Unlike traditional voltage-source and current-source inverters, the ZSI employs a unique impedance network that allows both voltage buck and boost operations within a single-stage power conversion structure. This feature makes it particularly attractive for renewable energy systems, where the input voltage can fluctuate significantly due to environmental conditions or load variations. Furthermore, the shoot-through state, which is normally prohibited in conventional voltage-source inverters, can be intentionally used in ZSI to boost the DC-link voltage without damaging the switching devices. Using ZSI, the functionalities of a boost converter and a voltage source inverter (VSI) can be integrated within a single-stage topology [5]. This capability reduces the need for an additional front-end DC-DC boost converter and consequently simplifies the overall power conversion structure. As a result, ZSI-based systems can achieve improved compactness, lower component count, and enhanced reliability compared with multi-stage converter configurations. ZSI are new generations of inverters that have introduced many advantages. These advantages include voltage boosting capability, improved immunity against shoot-through faults, wider input voltage operating range, and better suitability for renewable energy sources with fluctuating output voltage. A characteristic feature of this inverter is its impedance network, which is built from a pair of inductors and a pair of capacitors connected in an X style arrangement. This impedance network acts as an energy storage and transfer stage, enabling the inverter to boost the DC-link voltage during specific switching intervals. The inherent constraints associated with conventional VSIs and current-source inverters (CSIs) have been effectively eliminated in ZSI. In conventional VSIs, the shoot-through state must be strictly avoided because it can damage the switching devices, whereas in ZSI this state is intentionally utilized to achieve voltage boosting. Similarly, compared with CSIs, the ZSI provides more flexible operation and does not suffer from the same open-circuit limitations. Different methods of pulse width modulation (PWM) have been used in these inverters [6]. These modulation strategies directly influence the voltage gain, switching losses, harmonic performance, and stress imposed on passive and semiconductor components. Common PWM methods for ZSI include simple boost control, maximum boost control, maximum constant boost control, and space vector modulation-based techniques. Various applications of these inverters have been found in fuel cell battery [7], hybrid electric vehicles [8], charging a battery [9], photovoltaic (PV) systems [10], and wind energy conversion systems [11]. In these applications, the ability of ZSI to operate under a wide range of input voltage variations makes it particularly attractive. For example, in PV and fuel-cell systems, the source voltage may vary significantly due to environmental conditions, operating point changes, or load demand variations. Then, a suitable control strategy is necessary to handle the closed loop according to different applications. The control system must regulate the output voltage, DC-link voltage, capacitor voltage, inductor current, and injected grid current depending on the required operating mode. To this end, a comprehensive large-signal state-space averaged representation is needed [12]. Such a model provides a useful mathematical framework for analyzing the dynamic behavior of ZSI under both steady-state and transient operating conditions. Moreover, accurate modeling is essential for designing stable controllers, evaluating system performance, and predicting the influence of parameter variations on the converter response. Various control techniques, including both classical and nonlinear approaches, have been proposed in recent scientific publications for the regulation of ZSI systems [13]. Classical methods such as proportional-integral (PI) and proportional-integral-derivative (PID) controllers are widely used due to their simple structure and ease of implementation. However, nonlinear and advanced control techniques, including sliding mode control, model predictive control, feedback linearization, adaptive control, and robust control, have also been investigated to improve the dynamic response of ZSI-based converters. The main objective of these control approaches is to guarantee rapid transient behavior, accurate tracking performance, and tolerance to system parameter deviations [14,15]. In addition, an effective control strategy should ensure low output current distortion, stable operation under input voltage fluctuations, reduced sensitivity to load changes, and reliable performance during grid disturbances or renewable source intermittency.

Nevertheless, due to the nonlinear dynamics and the non-minimum phase characteristics of the ZSI topology, designing an appropriate control method remains a significant challenge. From a control system design perspective, the grid-connected single-phase ZSI configuration possesses two control inputs: the shoot-through duty cycle (STDC) and the amplitude modulation index. Conversely, the outputs to be regulated are the DC-link capacitor voltage and the grid-side AC current. Consequently, the ZSI constitutes a multi-input multi-output (MIMO) dynamic system, which inherently increases the complexity of the control design process. In many studies, small-signal linearization around a nominal operating condition has been employed to simplify the converter's nonlinear behavior. Ultimately, controllers are synthesized based on the resulting linearized system model for the selected steady-state condition. In [16], a proportional-resonant (PR) controller is proposed for managing the ZSI system. The key advantage of PR controllers lies in their capability to precisely follow sinusoidal reference signals with zero steady-state error. However, these controllers are typically developed utilizing the linearized representation of the ZSI, which limits their applicability over a broad range of operating scenarios. It has been demonstrated that the transfer function of the capacitor voltage exhibits a right half-plane (RHP) zero [17]. This causes it to become a nonminimum phase system. Therefore, it is not possible to directly control the capacitor voltage with the STDC, because it leads to instability of the system. A combined feedforward-feedback control was introduced in [18] to overcome the nonminimum phase of the studied system, while the value of the STDC is found based on the ideal model. Therefore, it becomes unreliable when the system operates under transient conditions.

In addition, the controller provided in a wide range of system operating points has errors. In [19], the AC and DC parts of controllers are designed separately. Therefore, the proposed controllers are not applicable. The nonlinear control methods proposed for the ZSI system in the articles include neural networks [20], fuzzy [21], model predictive control (MPC) [22], and sliding mode control (SMC) [23]. The predictive model control provides an efficient method in designing multi-input multi-output control systems. However, this controller lacks robustness with respect to system parameter fluctuations. SMCs feature a straightforward design structure and provide strong resilience against disturbances and uncertainties while delivering rapid dynamic behavior. These characteristics make SMCs preferable to neural network and fuzzy logic controllers. Nonetheless, SMCs are associated with certain disadvantages, such as chattering phenomena and variable switching frequencies. In [14], the SMC strategy is employed to regulate the DC-side variables (i.e., currents and voltages within the ZSI network), whereas the AC-side is controlled using a PI regulator. Linear controllers generally fail to accurately follow sinusoidal current references. Additionally, the methodology for determining the reference current of the DC-side inductors is not explicitly discussed. In [24], separate control schemes are applied for the DC and AC sides. However, this design approach entails complex analytical procedures.

The present research introduces an Interconnection and Damping Assignment Passivity-Based Control (IDA-PBC) strategy to regulate the grid-connected single-phase ZSI system. Compared to conventional methods in the literature, the proposed technique offers two major benefits. First, IDA-PBC provides enhanced transient behavior while guaranteeing the asymptotic convergence of system trajectories. Second, within the IDA-PBC framework, the Hamiltonian function is selected as a Lyapunov function candidate, thereby ensuring global stability guarantees. Since the control law is derived based on the nonlinear model of the converter, it can be effectively utilized under different operating situations. Simulation results confirm that the proposed IDA-PBC method ensures complete closed-loop stability and exhibits high robustness under variations in input voltage, DC-link reference voltage, and AC current references, all while achieving zero steady-state error.

2. Averaged state-space model of the ZSI

Figure 1 depicts the configuration of the ZSI, where the switching process is implemented using the PWM technique. To provide a clearer understanding of the converter operation, the associated switching states and their behavior are further examined in the following discussion with reference to Figure 2.

According to Figure 2, VCONTROL represents the inverter amplitude modulation index, while V_{tri} corresponds to the peak value of the triangular carrier signal. For the purpose of simplifying the mathematical model, a symmetry condition is assumed in the ZSI structure. Under this assumption, the two DC-side inductor currents are considered identical, and likewise, the voltages across the two DC-side capacitors are taken to be equal. As a result, the number of independent state variables associated with the DC side is reduced from four to two, which significantly simplifies the system representation and subsequent control design. In addition to these variables, the AC-side inductor current is selected as the third state variable. Accordingly, the state-variable vector can be defined as given in Equation (1).

$$X(t) = [i_{L_1} = i_{L_2}, V_{C_1} = V_{C_2}, i_{Ls}]^T = [x_1, x_2, x_3]^T \tag{1}$$

In Figure 1, Vi is the output voltage of the inverter in DC link and three operating conditions can be considered for this voltage.

Operating Mode 1: The output voltage of the inverter, V_{inv}, equals the DC-link voltage, V_{DC}, during the positive active switching interval $(0 < t < D_1T_s)$ i.e., $V_{inv} = V_{DC}$

Operating Mode 2: The output voltage, V_{inv}, equals the negative of the DC-link voltage during the negative active switching duration, $(D_1T_s < t < (D_1 + D_2)T_s)$ i.e., $V_{inv} = -V_{DC}$

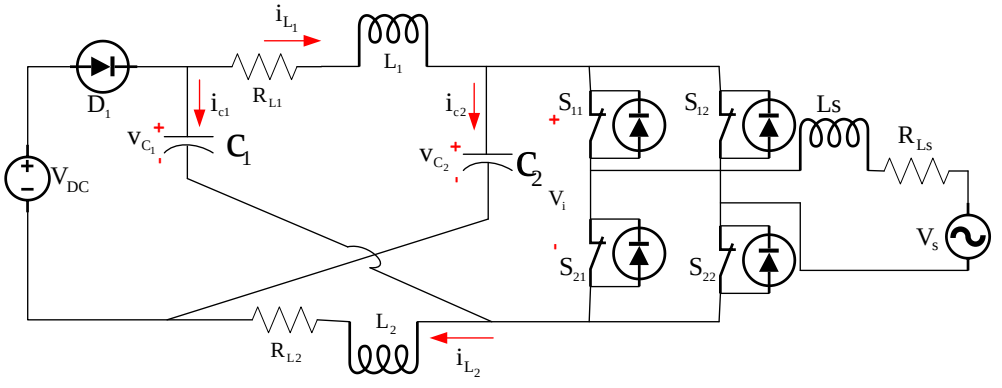

Figure 1. Configuration of a single-phase grid-connected ZSI.

Operating Mode 3: The inverter output voltage becomes zero throughout the shoot-through conduction phase, $((D_1 + D_2)T_s) < t < T_s$ i.e., $V_{inv} = 0$

Figure 3 shows the equivalent circuits of ZSI in different operating conditions. These equivalent circuits provide a clear description of the converter behavior under each switching state and are essential for understanding the dynamic operation of the system. In order to achieve the averaged state-space model, the state equations must be known for each operating condition. This is because the overall averaged model is obtained by combining the dynamics of all switching modes according to their corresponding duty ratios. Let's assume $L_1 = L_2 = L$ and $C_1 = C_2 = C$. These assumptions are typically introduced to simplify the mathematical derivation and to define the switching intervals more clearly within one switching period. In mode 1, S_{11} and S_{22} switches are turned ON, and the output voltage of the converter equals the input voltage. Under this condition, the power converter transfers energy in a direct manner from the source side to the load or grid side without applying any voltage boost effect through the impedance network. The equivalent circuit of the converter in this operating mode is illustrated in Figure 3(a). This circuit representation highlights the current paths through the inductors, capacitors, switching devices, and output stage during the first interval of operation. Based on the equivalent circuit configuration illustrated in Figure 3(a), the state-space representation of the grid-connected ZSI during the initial switching interval can be formulated as Equation (2).

$$\dot{X} = A_{on}X + B_{on}U = \begin{bmatrix} \frac{-R_{L1}}{L_1} & -\frac{1}{L_1} & 0 \\ \frac{1}{C_1} & 0 & -\frac{1}{C_1} \\ 0 & \frac{2}{Ls} & -\frac{R_{Ls}}{Ls} \end{bmatrix} X + \begin{bmatrix} \frac{1}{L_1} & 0 \\ 0 & 0 \\ -\frac{1}{Ls} & -\frac{1}{Ls} \end{bmatrix} \begin{bmatrix} V_{DC} \\ V_s \end{bmatrix} \tag{2}$$

This mathematical model describes the time evolution of the selected state variables and serves as the foundation for deriving the complete averaged dynamic model of the converter. Moreover, obtaining an accurate state-space equation for this mode is necessary for subsequent controller design, stability analysis, and dynamic performance evaluation.

During mode 2, switches S_{12} and S_{21} are turned ON, and under this switching state the converter output voltage becomes $-V_i$. In this operating condition, the switching configuration alters the conduction paths within the inverter bridge and consequently affects the voltage applied to the output terminals. As a result, the interaction between the inverter stage and the impedance network becomes different from that observed in the previous operating interval. The equivalent electrical circuit corresponding to this operating condition is presented in Figure 3(b). This circuit representation clearly illustrates the current paths through the inductors, capacitors, and switching devices when the converter operates in the second switching state. Based on this circuit configuration, the dynamic behavior of the grid-connected ZSI in the second switching interval can be described through the state-space model given in Equation (3). This mathematical formulation characterizes the evolution of the system state variables during this interval and contributes to the development of the overall averaged model of the converter.

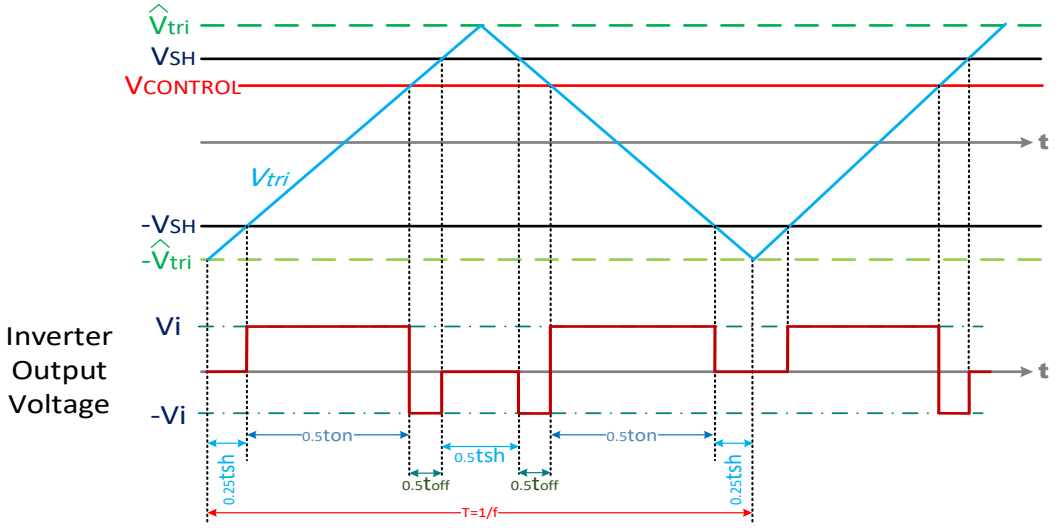

Figure 2. Switching pattern of the ZSI under PWM technique.

Finally, when the inverter operates in the shoot-through state (mode 3), the system dynamics change according to the corresponding switching pattern. In this particular operating mode, both switches of at least one inverter leg are intentionally turned ON simultaneously, creating the shoot-through condition that is normally avoided in conventional voltage source inverters. However, in the Z-source inverter topology, this state is deliberately utilized to boost the DC-link voltage by storing energy in the impedance network. Consequently, the voltages across the capacitors and the currents through the inductors exhibit distinct dynamic behavior during this interval. In this mode, the state-space equations of the converter are expressed as presented in Equation (4). The equivalent circuit associated with this operating interval, which helps illustrate the power flow path and the behavior of the impedance network, is shown in Figure 3(c). This representation highlights how the energy is transferred and temporarily stored within the Z-source network during the shoot-through period, enabling the voltage boosting capability that characterizes the ZSI topology.

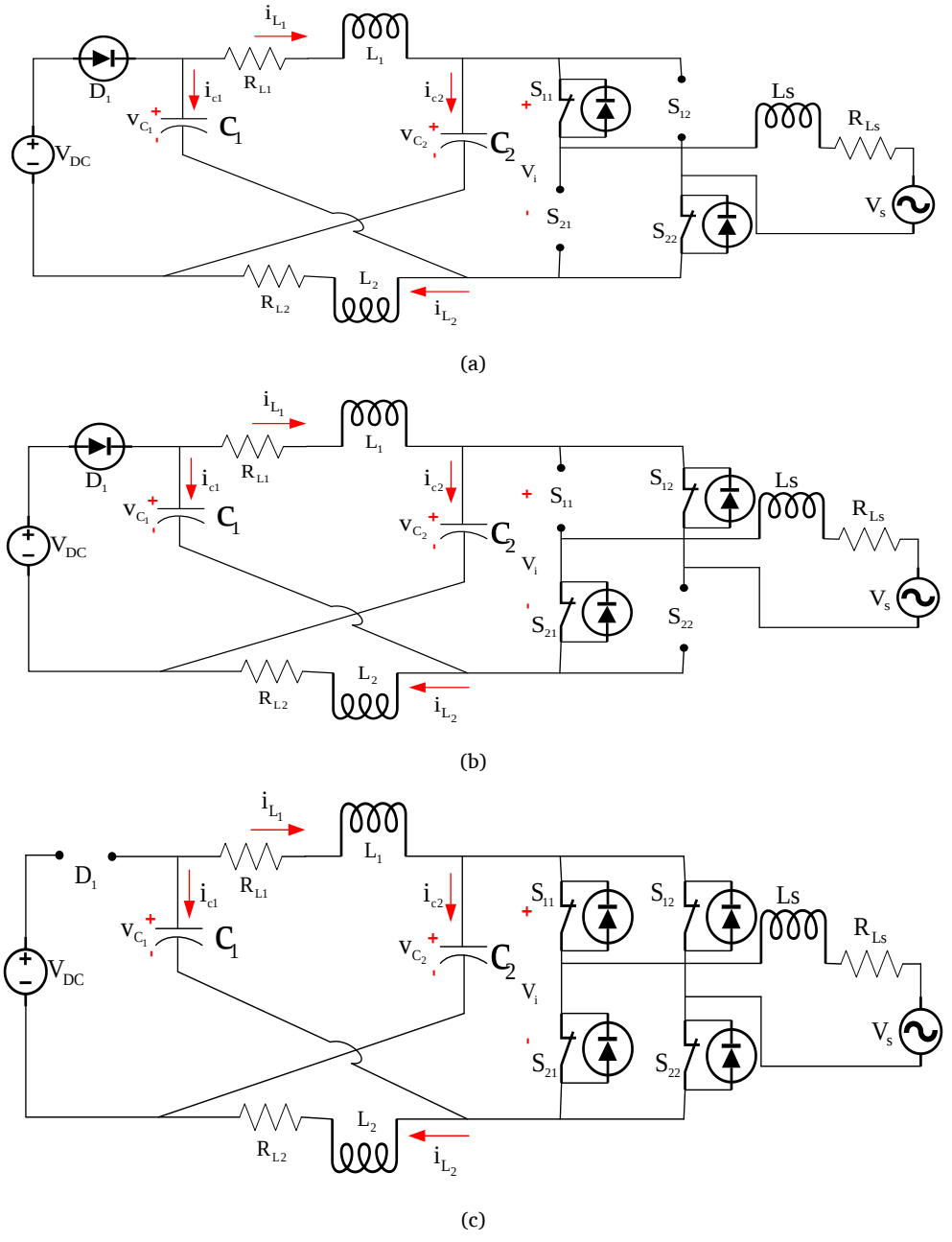

Figure 3. Equivalent of the ZSI during (a) Mode 1, (b) Mode 2, (c) Mode 3.

$$\dot{X} = A_{off}X + B_{off}U = \begin{bmatrix} \frac{-R_{L1}}{L_1} & -\frac{1}{L_1} & 0 \\ \frac{1}{C_1} & 0 & \frac{1}{C_1} \\ 0 & -\frac{2}{Ls} & -\frac{R_{Ls}}{Ls} \end{bmatrix} X + \begin{bmatrix} \frac{1}{L_1} & 0 \\ 0 & 0 \\ \frac{1}{Ls} & -\frac{1}{Ls} \end{bmatrix} \begin{bmatrix} V_{DC} \\ V_s \end{bmatrix} \tag{3}$$

$$\dot{X} = A_{sh}X + B_{sh}U = \begin{bmatrix} \frac{-R_{L1}}{L_1} & \frac{1}{L_1} & 0 \\ -\frac{1}{C_1} & 0 & 0 \\ 0 & 0 & -\frac{R_{Ls}}{Ls} \end{bmatrix} X + \begin{bmatrix} 0 & 0 \\ 0 & 0 \\ 0 & -\frac{1}{Ls} \end{bmatrix} \begin{bmatrix} V_{DC} \\ V_s \end{bmatrix} \tag{4}$$

To derive the final state-space equations of the converter, it is necessary to combine the models corresponding to the different operating modes, namely Equations (2)–(4). Since the Z-source inverter operates in multiple switching intervals within each switching period, the overall converter behavior cannot be accurately represented by a single mode alone. Instead, the complete dynamic model must be obtained by appropriately merging the state equations associated with each operating condition according to their respective durations. In this way, the influence of all switching states on the converter dynamics is taken into account in a unified mathematical framework. The switching intervals of the ZSI are shown in Figure 2. These intervals define the sequence and duration of the converter operating modes during one switching cycle and therefore play a key role in the averaging procedure. More specifically, the duty ratios associated with each mode determine the contribution of the corresponding state-space equations to the final averaged model. By using this information, the instantaneous switched model can be transformed into an averaged representation that is more convenient for analysis, simulation, and controller design. This averaged model preserves the essential dynamic characteristics of the original switched system while avoiding the complexity associated with direct switching behavior.

The state-space averaging technique commonly used in power electronic converters is presented in Equations (5)–(8).

$$\dot{X} = A_{ave}X + B_{ave}U \tag{5}$$

$$A_{ave} = \frac{1}{T}(t_{on}A_{on} + t_{off}A_{off} + t_{sh}A_{sh}) \tag{6}$$

$$B_{ave} = \frac{1}{T}(t_{on}B_{on} + t_{off}B_{off} + t_{sh}B_{sh}) \tag{7}$$

$$\begin{aligned} \frac{t_{on}}{T} &= \frac{u + 1 - d_{sh}}{2} \\ \frac{t_{sh}}{T} &= d_{sh} \\ \frac{t_{off}}{T} &= (1 - \frac{u + 1 - d_{sh}}{2} - d_{sh}) \end{aligned} \tag{8}$$

This method provides a systematic approach for deriving a continuous-time large-signal model from the discrete switching operation of the converter. In essence, the averaged state variables are obtained by weighting the dynamics of each switching mode with their respective duty cycles over a switching period. As a result, the final model becomes suitable for studying the low-frequency dynamic response of the system, designing control strategies, and evaluating stability under different operating conditions. Therefore, the application of the state-space averaging method is a fundamental step in the mathematical modeling of the grid-connected ZSI.

By substituting Equation (8) into Equations (6) and (7), the dynamic relations can be further simplified and rearranged into the final state-space representation of the system. Accordingly, the complete model of the converter is obtained in the form given by Equations (9) and (10).

$$A_{ave} = \begin{bmatrix} \frac{-R_{L1}}{L_1} & \frac{2d_{sh} - 1}{L_1} & 0 \\ \frac{1 - 2d_{sh}}{C_1} & 0 & \frac{-u}{C_1} \\ 0 & \frac{2u}{Ls} & \frac{-R_{Ls}}{Ls} \end{bmatrix} \tag{9}$$

$$B_{ave} = \begin{bmatrix} \frac{1}{L_1}(1 - d_{sh}) & 0 \\ 0 & 0 \\ \frac{-u}{Ls} & \frac{-1}{Ls} \end{bmatrix} \tag{10}$$

From a control point of view, the single-phase grid-connected Z-source inverter can clearly be regarded as a MIMO system. This classification arises from the fact that the converter includes more than one independent control input and more than one output variable that must be regulated simultaneously.

In such a system, the internal dynamics are strongly coupled, meaning that a change in one control input may influence several state variables at the same time. Therefore, an effective controller must be designed by taking these interactions into account rather than treating each variable independently.

The two manipulated variables of the system are the amplitude modulation index and the STDC, denoted by d_{sh} and u, respectively. The amplitude modulation index primarily governs the AC-side behavior of the inverter and directly affects the magnitude of the output voltage or injected current. On the other hand, the shoot-through duty cycle plays a key role in regulating the boosting action of the Z-source network by determining the duration of the shoot-through interval within each switching period. Through proper adjustment of these two control inputs, it becomes possible to manage both the DC-side and AC-side performance of the converter in a coordinated manner. This dual-input characteristic is one of the main distinguishing features of the ZSI when compared with conventional inverter topologies.

Additionally, the DC-link capacitor voltage and the inverter's AC output current constitute the system's controlled variables. These variables are of primary importance because they reflect the energy balance and power transfer capability of the converter. The DC-link capacitor voltage must be maintained around its desired reference value to ensure sufficient energy storage and stable converter operation, while the AC output current must accurately track its reference in order to achieve proper grid power injection with acceptable dynamic and steady-state performance. Since both outputs are interconnected through the converter dynamics, the regulation problem becomes more challenging and requires a control strategy capable of handling the inherent coupling and nonlinear behavior of the system. For this reason, modeling the grid-connected single-phase ZSI as a MIMO system provides a more realistic and effective basis for control design and stability analysis.

3. Port-Controlled Hamiltonian System (PCHS)

The model of the single-phase grid-connected ZSI is developed here based on PCHS. According to theory of PCHS, dynamic systems with energy storage elements is described as Equation (11).

$$\dot{X} = [J(x,u) - R(x)]\frac{\partial H(x)}{\partial x} + g(x,u) \tag{11}$$
$$y = g^T(x)\nabla H(x)$$

u, x and y are the control, state, and output variables of the system, respectively. y and u are called port variables and the product of these two variables shows the power injected into the system. In Equation (12), $H(x): R^n \to R$ is the Hamilton function (energy function) in which the following conditions should be met: $H(0) = 0$ and $x \neq 0, H(x) > 0$. Also $J(x) \in R^{n\times n}$ is the interconnection matrix and $R(x) \in R^{n\times n}$ is the damping or dissipation matrix. The following relationships must be established for these matrices:

$$J(x) = -J^T(x) \tag{12}$$
$$R(x) = R^T(x) \geq 0$$

In Equation (11), $g \in R^{n\times m}$ is the kernel of the systems input matrix. It is widely recognized that passivity plays a fundamental role in ensuring system stability. A system qualifies as passive if the energy delivered to it over a specified period is at least equal to the energy it retains. Mathematically, this property is shown in Equation (13):

$$\frac{dH(x)}{dt} = (\frac{\delta H(x)}{\delta x})^T \dot{x} = -(\frac{\delta H(x)}{\delta x})^T R(x)(\frac{\delta H(x)}{\delta x}) + u^T y \leq u^T y \tag{13}$$

Two basic and important characteristics of PCHS systems are their inherent inactivity and their stability. Equation (13) indicates that the energy accumulated within a passive system does not exceed the externally delivered energy. In other words, a passive system is unable to generate energy. By integrating Equation (13), the energy balance equation is obtained as Equation (14).

$$\underbrace{H[x(t)] - H[x(0)]}_{Stored} = \underbrace{\int_0^t u^T(s)y(s)ds}_{Supplied} - \underbrace{\int_0^t (\frac{\partial H[x(s)]}{\partial x})^T R[x(s)](\frac{\partial H[x(s)]}{\delta x})ds}_{dissipated} \tag{14}$$

According to Equation (14), it can be concluded that $H[x(t)] \leq H[x(0)]$. This indicates that, because of the dissipative nature of the system, the stored energy gradually decreases over time and eventually vanishes when the system reaches its minimum-energy state. From a control perspective, however, the goal is not merely to let the system settle at this trivial energy minimum, but rather to drive and maintain it around a meaningful equilibrium point that corresponds to the desired operating condition. In other words, the controller must shape the system dynamics in such a way that the energy behavior supports stable operation in the vicinity of a specified non-zero equilibrium.

3.1. PCHS modelling

To develop a passivity-based control scheme, the state-space representation of the system must first be transformed into the structure illustrated in Equation (11). For this purpose, by placing A_{avg} (Equation (9)) and B_{avg} (Equation (10)) in Equation (5), the closed-form expression for $\dot{X}$ is obtained.

By comparing this expression with Equation (11), matrices J, R and g are obtained as Equation (15):

$$J(x,u)=\begin{bmatrix} 0 & \frac{2d_{sh}-1}{LC} & 0 \\ \frac{1-2d_{sh}}{LC} & 0 & \frac{-u}{(Ls)(C)} \\ 0 & \frac{u}{(Ls)(C)} & 0 \end{bmatrix}, R(x)=\begin{bmatrix} \frac{R_{L1}}{L^2} & 0 & 0 \\ 0 & 0 & 0 \\ 0 & 0 & \frac{R_{Ls}}{(Ls)^2} \end{bmatrix}, g=\begin{bmatrix} \frac{(1-d_{sh})V_{DC}}{L} \\ 0 \\ \frac{u(x_2-V_{DC})-V_s}{Ls} \end{bmatrix} \tag{15}$$

3.2. IDA-PBC theory

The IDA-PBC method is widely regarded as an effective nonlinear control approach for systems that are represented in the PCH form. The main idea behind this strategy is to redesign the system dynamics so that a desired equilibrium point x_d is achieved through the construction of an appropriate target energy function. This objective is accomplished by properly shaping the interconnection matrix $J_d(x)$, the damping matrix $R_d(x)$, and the control input in a coordinated manner. By modifying these structural elements, the controller is able to influence both the energy distribution and the dissipative behavior of the system, thereby enforcing the desired closed-loop performance.

In addition to energy shaping, another important purpose of the IDA-PBC framework is to derive a suitable state-feedback control law $u(x)$ for the system expressed in the PCH structure. This feedback signal is designed such that the closed-loop dynamics satisfy the required stability and convergence properties, as described in Equation (16). In this way, the controller not only stabilizes the system around the selected operating point but also ensures that the system trajectories evolve toward the intended equilibrium in a systematic and theoretically grounded manner.

$$\dot{x}=[J_d(x)-R_d(x)]\frac{\partial H_d(x)}{\partial x} \tag{16}$$

with

$$\begin{aligned} &J_d(x)=[J(x)+J_a(x)]=-J_d^T(x), \\ &R_d(x)=[R(x)+R_a(x)]=R_d^T(x)\geq 0, \\ &H_d(x)=[H(x)+H_a(x)]\geq 0 \end{aligned} \tag{17}$$

In Equations (16) and (17), the functions and matrices denoted with the subscript d represent their desired or target counterparts in the closed-loop system (CLS). In this framework, the modified energy function, expressed as Hd(x), is constructed such that it possesses a minimum ($H(\tilde{x})=\arg\min H_d(x)$) at the desired equilibrium point $\tilde{x}$, where $\tilde{x}\in R^n$. This equilibrium point corresponds to the operating condition at which the system is intended to be stabilized through the proposed control design.

Within the IDA-PBC methodology, the control objective is not limited to defining a new energy function. In addition to reshaping the energy of the system, appropriate desired interconnection and damping matrices are also introduced to modify the natural dynamic behavior of the open-loop model. As a result, the original open-loop energy function is systematically converted into a closed-loop energy function according to the relation presented in Equation (17). This transformation allows the CLS to exhibit the desired stability properties around the selected equilibrium point.

Furthermore, the terms $H_a(x)$, $J_a(x)$, and $R_a(x)$ correspond to the injected function and injected matrices required for energy shaping and damping assignment. These injected components are defined in detail in Equations (19) and (20) and are used to adjust the system structure so that the resulting closed-loop dynamics satisfy the intended performance and stability requirements.

$$J_a(x)=-J_a{}^T(x) \tag{18}$$

$$R_a(x)=R_a{}^T(x) \tag{19}$$

$$H_a(x)=H_a{}^T(x) \tag{20}$$

The matrices $J_a(x)$ and $R_a(x)$ are assumed to be skew-symmetric and positive semi-definite, respectively, in accordance with the physical properties of the system. To compute the appropriate interconnection and dissipation matrices for the closed-loop dynamics, $J_a(x)$ and $R_a(x)$ are formulated in line with Equation (17). Based on Equations (11) and (16), the resulting expression can be obtained as Equation (21):

$$[J(x,u)-R(x)]\frac{\partial H(x)}{\partial x}+g(x,u)=[J_d(x)-R_d(x)]\frac{\partial H_d(x)}{\partial x} \tag{21}$$

3.3. Controller design based on IDA-PBC

In this part, the structure of interconnection and damping matrices is formulated to achieve the predefined control objectives. Let $x_{id}(i=1,2,3)$ denote the target steady-state conditions of the CLS. The energy function of the desired closed-loop dynamics is expressed as Equation (22):

$$H_d(x)=\frac{1}{2}L(x_1-X_{1d})^2+\frac{1}{2}C(x_2-X_{2d})^2+\frac{1}{2}L_s(x_3-X_{3d})^2 \tag{22}$$

In Equation (22), voltage of the capacitors on the DC-side (x2) and AC-current injected to network (x3) are selected based on the desired values, which are specified by index d. At the system's equilibrium condition, the state-space dynamics are assumed to approach zero. By calculating the control variables, the value of the DC-inductor reference current is expressed as Equation (23):

$$X_{2d} = V_{ref}$$
$$X_{3d} = I_{Lsref} \quad (23)$$
$$X_{1d} = \frac{V_{DC} - \sqrt{V_{DC}^2 - 8R_L(x_3V_s + x_3^2R_{Ls})}}{4R_L}$$

The interconnection and damping matrices are taken into account in Equation (24).

$$J_a = 0 \in R^{3\times3}$$
$$R_a = diag[r_1\ r_2\ r_3] \quad (24)$$

Therefore, the desired damping and interconnection matrices can be defined as Equations (25) and (26):

$$R_d = diag[r_1 + \frac{R_{L1}}{L^2}, r_2, r_3 + \frac{R_{Ls}}{(Ls)^2}] \quad (25)$$
$$J_d = J_a \quad (26)$$

Following straightforward analytical manipulations, the resulting scalar differential equations are obtained as Equation (27):

$$(-r_1L - \frac{R_{L1}}{L})x_{1d} + (\frac{2d_{sh}-1}{L})x_{2d} = \frac{d_{sh}-1}{L}V_{DC} - r_1Lx_1 \quad (27)$$
$$(\frac{2d_{sh}-1}{C})x_{1d} + r_2Cx_{2d} + (\frac{u}{C})x_{3d} = r_2Cx_2$$
$$(\frac{u}{Ls})x_{2d} + (-r_3(Ls) - \frac{R_{Ls}}{L_s})x_{3d} = -r_3(Ls)x_3 + \frac{uV_{DC} - ux_2 + V_s}{(Ls)}$$

Using Equation (27), the ZSI inverter control commands d_{sh} and u are obtained as Equations (28) and (29):

$$d_{sh} = \frac{-r_1L^2x_1 - V_{DC} + x_{2d} + x_{1d}r_1L^2 + R_{L1}x_{1d}}{2x_{2d} - V_{DC}} \quad (28)$$

$$u = \frac{x_{3d}(Ls)(r_3(Ls) + \frac{R_{Ls}}{Ls}) + V_s - r_3(Ls)^2x_3}{x_{2d} + x_2 - V_{DC}} \quad (29)$$

Figure 4 depicts a block diagram of the suggested method.

3.4. Proof of stability

To examine the stability properties of the developed control scheme, the closed-loop Hamiltonian function is defined and adopted $H_d(x)$ as a Lyapunov candidate function. In the framework of PBC, the Hamiltonian represents the total stored energy of the system. Therefore, by analyzing its evolution over time, it becomes possible to assess whether the controlled system remains stable and converges toward the desired operating point. In this study, the closed-loop energy function is selected because it provides a physically meaningful and mathematically suitable basis for stability analysis.

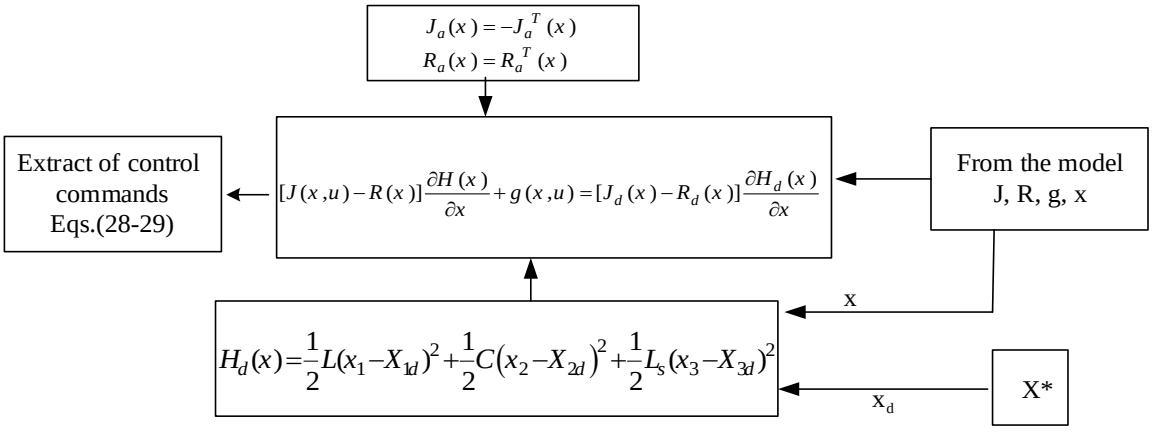

Figure 4. Schematic of the control method used.

Accordingly, the time derivative of the closed-loop Hamiltonian is computed along the trajectories of the CLS, and the resulting expression is given in Equation (30):

$$V = H_d(x) = (x - x_d)^T Q(x - x_d)$$
$$\dot{V} = \dot{H}_d = (\nabla H_d(x))^T \dot{x} = \{\nabla H_d(x)\}^T \{J_d(x) - R_d(x)\} \{\nabla H_d(x)\} \quad (30)$$

The sign of this derivative plays a fundamental role in determining the stability behavior of the system. If the derivative of the Hamiltonian is non-positive, then the total system energy does not increase with time, which directly supports the stability of the closed-loop dynamics.

Within the PCH structure, the interconnection matrix $J_d(x)$ possesses a skew-symmetric property. Owing to this characteristic, the term associated with the interconnection matrix does not contribute to any net increase or decrease in the system energy. In other words, it only redistributes energy among the internal states without generating or dissipating it. Based on this important property, the relation expressed in Equation (31) is obtained:

$$\{\nabla H_d(x)\}^T J_d(x) \{\nabla H_d(x)\} = 0 \quad (31)$$

Furthermore, the damping matrix $R_d(x)$ is assumed to be positive semi-definite. This property ensures that the damping term always contributes to energy dissipation or, at minimum, does not inject energy into the system. As a consequence, the expression given in Equation (32) can be established:

$$\dot{V} = \dot{H}_d(x) = -\{\nabla H_d(x)\}^T R_d(x) \{\nabla H_d(x)\} < 0 \quad (32)$$

From Equations (30)–(32), it follows that the time derivative of the closed-loop Hamiltonian $H_d(x)$ is always less than or equal to zero. This result implies that the closed-loop energy function is a non-increasing function of time. Therefore, according to Lyapunov stability theory, the Hamiltonian satisfies the required conditions to be considered a valid Lyapunov candidate function $V > 0, \dot{V} < 0$. Since the stored energy of the system continuously decreases, or at least does not increase, the system states remain bounded and move toward the equilibrium condition.

As time progresses, the dissipative effect introduced by the damping structure causes the system energy to decrease gradually until the system reaches its minimum-energy configuration. This minimum corresponds to the desired equilibrium point defined in the controller design. Consequently, the proposed CLS is not only stable in the Lyapunov sense, but also asymptotically stable, because the state trajectories converge to the desired equilibrium as time tends to infinity.

It is important to note that, in the IDA-PBC approach, the stability of the system is achieved through both energy shaping and damping injection. The energy shaping process constructs a desired Hamiltonian function whose minimum is located at the selected equilibrium point, while the damping injection mechanism ensures that the system energy decreases over time. The combination of these two actions gives the controller a strong theoretical foundation and guarantees stable operation under the designed conditions.

In addition to the analytical proof, the practical implementation of the presented control strategy is illustrated in Figure 5, where the converter is controlled through the generated switching signals. This figure shows how the control law is translated into an actual switching pattern for the power converter. More specifically, the switching signals determine the operating states of the converter in such a way that the desired energy behavior and dynamic response are achieved. Hence, Figure 5 provides a practical representation of how the theoretical control design is applied in the converter structure.

Overall, the presented stability analysis confirms that the proposed control strategy ensures a stable closed-loop response by enforcing a monotonic decrease in the system energy. The use of the closed-loop Hamiltonian as a Lyapunov function, together with the skew-symmetric property of the interconnection matrix and the positive semi-definite nature of the damping matrix, provides a rigorous justification for the asymptotic stability of the controlled converter system.

4. Simulation

To assess both the steady-state behavior and the dynamic response of the presented control methods, a series of simulation studies is carried out on a grid-connected single-phase ZSI. The electrical parameters of the inverter as well as the tuning parameters of the implemented controllers, together with their numerical values, are reported in Table 1. All simulation analyses were conducted within the MATLAB/Simulink platform, specifically version 2018.

Table 1 summarizes the principal electrical parameters of the grid-connected single-phase ZSI system together with the main controller settings used in the simulation studies. These parameters define the operating conditions of the converter and are selected to assess the performance of the control method.

The input DC power source is set to 100 V, which provides the primary energy required for the inverter operation. On the grid side, the utility voltage has a peak value of 110 V, representing the AC grid to which the inverter is connected.

The impedance network of the ZSI includes DC-side inductors with an inductance value of 1.6 mH, each having an equivalent series resistance of 0.08 Ω. These inductors are responsible for energy storage and play an important role in shaping the dynamic behavior of the converter. In addition, the DC-side capacitors have a capacitance value of 1 mF, which contributes to stabilizing the DC-link voltage and maintaining proper operation of the impedance network.

On the AC side of the inverter, a coupling inductor of 3 mH is used to connect the inverter output to the grid. This inductor limits current ripple and facilitates smooth current injection into the grid. The equivalent resistance associated with the AC-side inductor is 0.012 Ω, which represents the practical resistive losses present in the inductor.

For the control objectives, the reference voltage of the DC-link capacitor is specified as 400 V, which determines the desired operating level of the DC-link. Furthermore, the reference peak value of the inverter output current injected into the grid is set to 20 A, ensuring that the inverter delivers the required current while remaining synchronized with the grid voltage.

Finally, Table 1 also includes the damping matrix parameters and the index used in the controller formulation, which are required in the implementation of the IDA-PBC control method. These parameters are employed to shape the system energy and introduce the necessary damping to guarantee stable and robust operation of the converter. Overall, the parameters listed in Table 1 establish the electrical characteristics of the ZSI system and provide the necessary values for conducting the simulation analysis presented in this study.

In this study, the DC-link capacitor voltage and the AC current delivered to the grid are selected as the main output variables for performance evaluation. These quantities are used to examine how effectively the control schemes regulate the inverter and maintain the desired operating conditions under different scenarios. It should also be noted that, throughout the simulation process, the parasitic components of the converter were neglected in order to simplify the model and focus on the principal dynamic characteristics of the system.

4.1. Varying Steady-State Conditions

Using the system parameters listed in Table 1, the dynamic and steady-state performances of the proposed controller are evaluated. Figure 6 illustrates the waveforms of the DC-link capacitor voltage, the AC current delivered to the grid, and the current tracking error, which is defined as the deviation between the reference grid current and the measured injected current. For this test condition, the reference voltage assigned to the DC-side capacitor is chosen as 400 V. In addition, the amplitude of the sinusoidal grid current reference is fixed at 20 A, while its phase is synchronized with the utility grid voltage to ensure unity power factor operation.

The results shown in Figure 6 indicate that the DC-link capacitor voltage successfully converges to its prescribed value and remains accurately regulated around 400 V during steady-state operation. No noticeable residual error is observed in the voltage response, confirming the effectiveness of the voltage regulation loop. Furthermore, the actual injected grid current closely follows its reference trajectory, and the corresponding tracking error remains very close to zero. This small deviation confirms that the controller can achieve high-quality current tracking and accurate power injection into the grid.

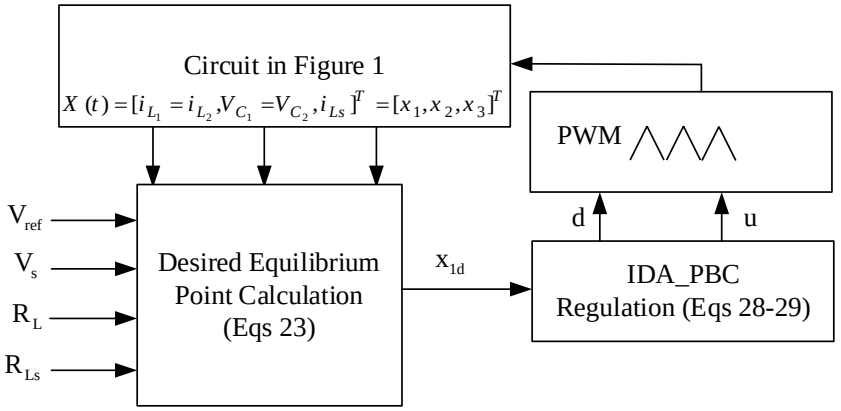

Figure 5. Control method used with switching.

Table 1. ZSI and IDA-PBC Parameters Specification.

Description	Parameter	Value
Input direct current (DC) Power source	V_{DC}	100v
Utility voltage(peak)	V_s	110v
DC-side inductors	$L_1 = L_2$	1.6mH
Equivalent resistance of DC-side inductors	$R_{L1} = R_{L2}$	0.08 Ω
DC-side capacitors	$C_1 = C_2$	1mf
Alternating current (AC) coupling inductor	Ls	3mH
Equivalent resistance of AC-side inductors	R_{Ls}	0.012 Ω
dc- link reference voltage	V_{ref}	400v
Reference current of the ZSI output (peak)	I_{Lsref}	20A
Damping matrix Index	r_1, r_2, r_3	$10^{-3}, 0, \frac{1}{L_s^4}$

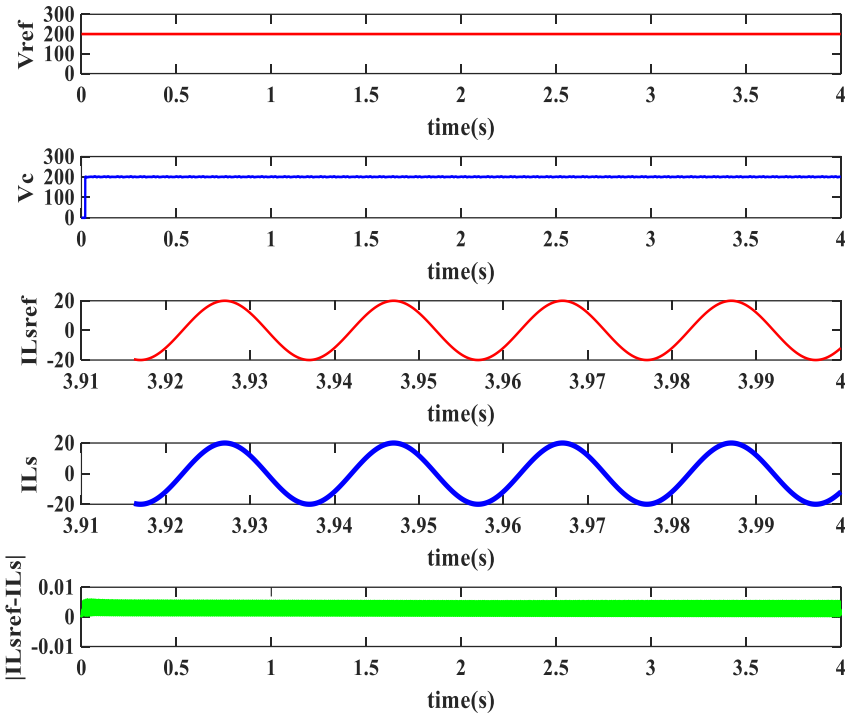

Figure 6. IDA-PBC performance under steady-state conditions.

These simulation results clearly verify the capability of the proposed control scheme to provide reliable steady-state operation and precise reference tracking. The negligible error between the desired and actual current waveforms also demonstrates the robustness of the controller against normal operating variations. Consequently, the proposed strategy ensures stable closed-loop behavior, accurate regulation of the DC-link capacitor voltage, and zero steady-state tracking error for the grid-side current.

4.2. Varying Input Voltage

In this test scenario, the inverter begins operating under its nominal conditions. To validate the robustness of the developed controller against input disturbances, a step change is applied at t = 2 s, where the input voltage is altered from its initial nominal value to 50 V. This variation is introduced to evaluate the controller's ability to preserve system stability and acceptable performance when the source voltage undergoes a sudden change.

As per Figure 7, the controller maintains a stable response throughout the disturbance period. Also, both the DC-link voltage tracking performance and the grid-side current regulation remain highly accurate, with the steady-state error remaining approximately zero. In addition, the transient response following the applied voltage step is satisfactory, indicating that the controller is able to quickly adapt to the new operating condition without causing instability or significant oscillations.

Therefore, these results confirm that the proposed control strategy preserves closed-loop stability under variations in the input voltage and provides an acceptable dynamic performance during transient conditions.

4.3. Varying Grid-Side AC Reference Current

In this scenario, the inverter initially operates under nominal conditions. After the system reaches a steady-state operating point, a step change is applied at t = 2 s, where the amplitude of the grid-side AC reference current is increased from 20 A to 25 A. During this evaluation, the reference voltage of the DC-link capacitor is kept constant at 200 V in order to examine the controller's capability to regulate the system while the current demand changes.

Based on the simulation results presented in Figure 8, the IDA-PBC controller maintains a stable and well-regulated system response despite the imposed variation in the reference current. The results indicate that the proposed control strategy exhibits strong robustness against changes in the operating conditions of the ZSI. Furthermore, the tracking performance of the grid-side current remains highly accurate, as the deviation between the reference current and the actual current injected into the grid remains practically zero. These observations confirm the effectiveness of the controller in handling variations in current demand while preserving stable system operation.

4.4. Varying DC-Link Capacitor Voltage Reference

In this scenario, the stability and robustness of the designed IDA-PBC controller are evaluated under variations in the reference voltage of the DC-link capacitor. Initially, the inverter operates under nominal operating conditions. At t = 2 s, a step change is applied to the DC-link voltage reference, increasing it from 200 V to 250 V in order to assess the controller's ability to adapt to reference modifications.

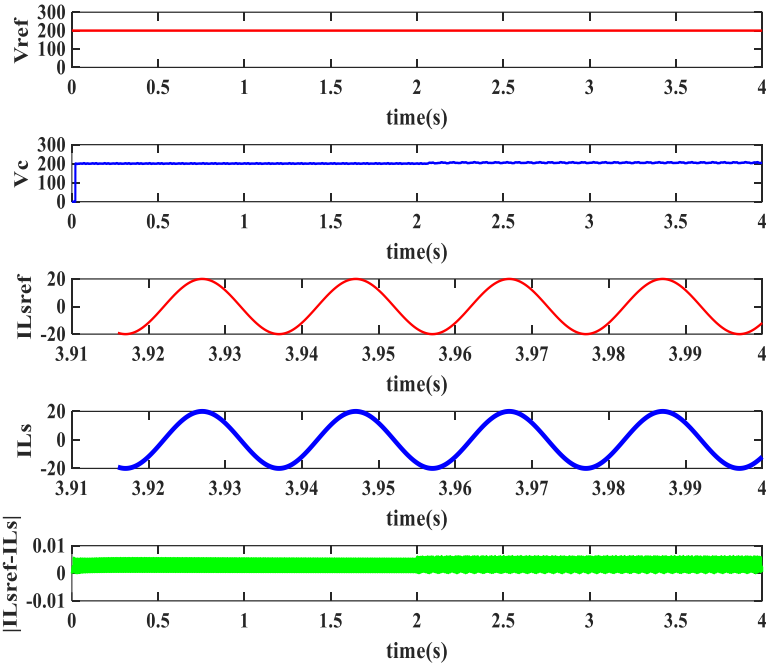

Figure 7. IDA-PBC response to input voltage step change (100V → 50V).

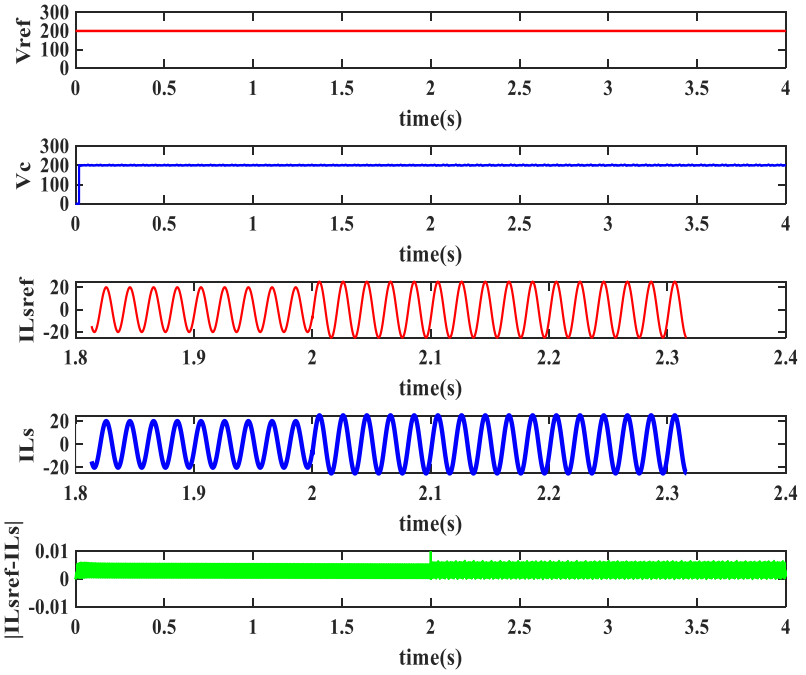

Figure 8. IDA-PBC response to grid current step change (20A → 25A).

The transient response of the control method during this change is depicted in Figure 9. It is seen that the controller effectively regulates the DC-link capacitor voltage and quickly guides the system toward the new operating point. Furthermore, the results demonstrate that the steady-state error is practically negligible, while the overall system response remains stable throughout the transition. These observations confirm that the IDA-PBC-based controller maintains reliable operation and robust performance when the DC-link voltage reference is varied, ensuring accurate voltage regulation and stable converter behavior.

4.5. Varying input voltage, output side reference current and dc side reference voltage

For this purpose, the simulation is carried out by changing the inverter operating conditions from 200 V, 20 A, 100 V to 250 V, 25 A, 50 V. These variations correspond to simultaneous changes in the output-side reference current, the DC-side reference voltage, and the input voltage, respectively. Such a wide-range disturbance allows the robustness and dynamic capability of the controller to be evaluated in a more rigorous manner.

Based on the responses shown in Figure 10, the controllers preserve a stable dynamic behavior despite the significant parameter variations applied to the system. The control strategy is capable of regulating both voltage and current effectively, even after relatively large changes are imposed on the operating conditions. In other words, the controller successfully maintains the system outputs close to their desired reference values, confirming its robustness, stability, and satisfactory transient performance under simultaneous disturbances.

5. Conclusions

This work introduces a MIMO control scheme based on the IDA-PBC methodology for a single-phase ZSI operating in grid-connected mode. To establish the theoretical background, the fundamental principles of the IDA-PBC framework are briefly revisited, emphasizing its suitability for nonlinear power electronic systems. The proposed control architecture is designed to simultaneously coordinate the dynamic behavior of both the DC-side and AC-side states of the inverter, ensuring proper power exchange with the utility grid. Within the control structure, independent regulation of the grid-side current and the DC-link capacitor voltage is achieved by manipulating two key control inputs: the amplitude modulation index, which governs AC-side current shaping, and the STDC, which directly influences the DC-link voltage dynamics. The overall stability of the CLS is demonstrated through a rigorous Lyapunov-based analysis, confirming that the controller enforces asymptotic tracking and ensures convergence of the system states under nominal conditions. Simulation studies were performed to examine the performance of the proposed scheme. According to these results, the IDA-PBC approach maintains an almost negligible steady-state error across a broad range of operating scenarios and achieves a fast transient response, highlighting its effectiveness for real-time grid-integration tasks.

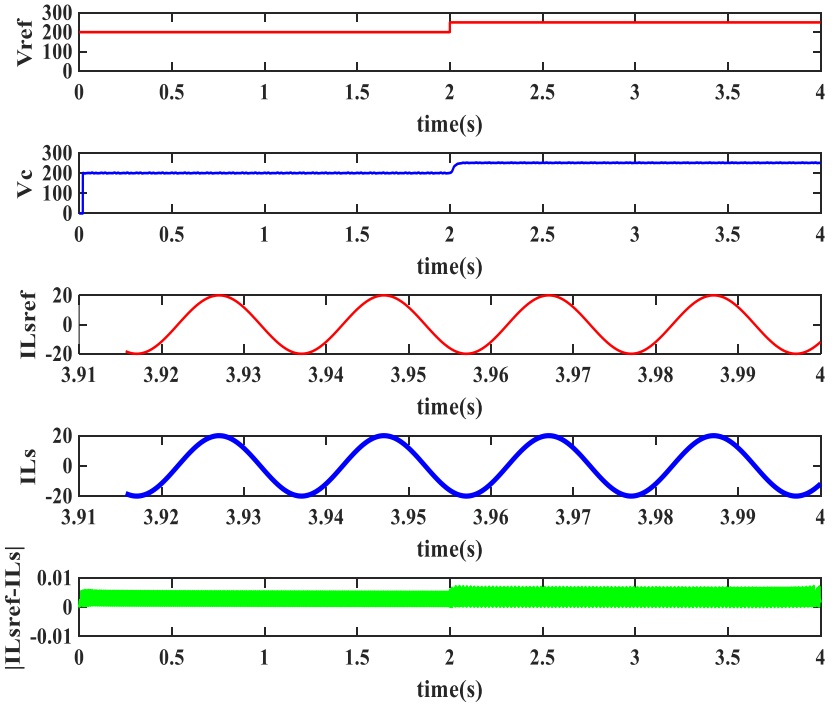

Figure 9. IDA-PBC response to DC link voltage step change (200V → 250V).

However, it is important to acknowledge that the presented simulations do not include the influence of parasitic components, such as inductor resistances or capacitor equivalent series resistance, which can affect the dynamic characteristics of practical implementations. Moreover, variations in inverter parameters were not explicitly modeled, and the controller was evaluated under idealized component values. These simplifications outline potential directions for future work, where incorporating parasitic effects, parameter uncertainties, and more realistic system disturbances could further refine the controller's robustness and enhance the accuracy of performance predictions.

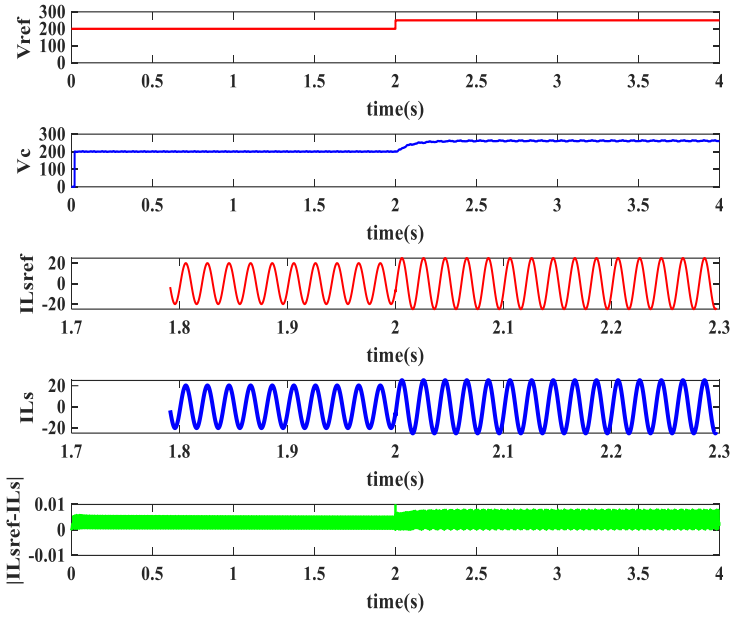

Figure 10. IDA-PBC response to step changes in grid current, input voltage, and DC capacitor voltage.

Nomenclature

Symbol	Description
x	System state vector
x_1, x_2, x_3	Individual state variables
$u \in \{on, off, short, avg\}$	Switching states of the inverter
B_1, B_2	Input matrices
i_1, i_2	Currents through the DC side inductors
i_{c1}, i_{c2}	Currents through the DC side capacitors
V_{c_1}, V_{c_2}	Voltage across the DC side capacitors
i_{L_1}, i_{L_2}	Currents through the AC side inductors
R_{L1}, R_{L2}	Equivalent series resistance of the DC side inductors
L_1, L_2	Inductance of the DC side inductors
C_1, C_2	Capacitance of the DC side capacitors
L_s	Inductance of the AC side inductor
R_{Ls}	Equivalent resistance of the AC side inductor
V_{DC}	Input DC voltage
V_s	Grid voltage
d_{sh}	Duty cycle of the shoot-through interval
u	Inverter AC side control signal
T	Switching period

References

[1] S. Padmanaban, P. K. Maroti, et al., "Quazi Z-Source Single Stage High Step-Up DC-DC Converter for Grid-Connected PV Application," *2019 IEEE International Conference on Environment and Electrical Engineering and 2019 IEEE Industrial and Commercial Power Systems Europe (EEEIC / I&CPS Europe)*, pp. 1–6, 2019.

[2] P. Padmavathi, and S. Natarajan, "Single Switch Quasi Z-source Based High Voltage Gain DC-DC Converter," *International Transactions on Electrical Energy Systems*, vol. 30, no. 7, 2020.

[3] X. ZHU, and B. ZHANG, "High Step-Up Quasi-Z-Source DC–DC Converters with Single Switched Capacitor Branch," *Journal of Modern Power Systems and Clean Energy*, vol. 5, no. 4, pp. 537–547, 2017.

[4] Fang Zheng Peng, "Z-Source Inverter," *IEEE Transactions on Industry Applications*, vol. 39, no. 2, pp. 504–510, 2003.

[5] Y. Liu, H. Abu-Rub, B. Ge, F. Blaabjerg, O. Ellabban, and P. C. Loh, *Impedance Source Power Electronic Converters*, John Wiley & Sons, 2016.

[6] P. C. Loh, F. Blaabjerg, and C. P. Wong, "Comparative Evaluation of Pulse-Width Modulation Strategies for Z-Source Neutral-Point-Clamped Inverter," *2006 37th IEEE Power Electronics Specialists Conference*, pp. 1–7, 2006.

[7] A. Behdani, and M. R. Naseh, "Power Management and Nonlinear Control of a Fuel Cell–Supercapacitor Hybrid Automotive Vehicle with Working Condition Algorithm," *International Journal of Hydrogen Energy*, vol. 42, no. 38, pp. 24347–24357, 2017.

[8] M. R. Naseh, and A. Behdani, "Non-Linear Control of Fuel Cell/Ultra-Capacitor Hybrid Electric Vehicle Using Comprehensive Function Algorithm Based on IDA-PBC," *Advanced Energy Conversion Materials*, pp. 1–17, 2023.

[9] G. R. Shahabadi, M. R. Naseh, and S. Eshaghi, "Non-Linear Control of Quasi-Z-Source Inverter with Battery for Renewable Energy Systems Based on Interconnection-Damping-Assignment Passivity-Based Control," *Journal of Applied Dynamic Systems and Control*, vol. 1, no. 3, p. 17, 2023.

[10] J. Liu, J. Wu, J. Qiu, and J. Zeng, "Switched Z-Source/Quasi-Z-Source DC-DC Converters With Reduced Passive Components for Photovoltaic Systems," *IEEE Access*, vol. 7, pp. 40893–40903, 2019.

[11] S. Dehghan, M. Mohamadian, and A. Varjani, "A New Variable-Speed Wind Energy Conversion System Using Permanent-Magnet Synchronous Generator and Z-Source Inverter," *IEEE Transactions on Energy Conversion*, vol. 24, no. 3, pp. 714–724, 2009.

[12] M. K. Kazimierczuk, "Small-Signal Modeling of Open-Loop PWM Z-Source Converter by Circuit-Averaging Technique," *IEEE Transactions on Power Electronics*, vol. 28, no. 3, pp. 1286–1296, 2013.

[13] G. R. Shahabadi and M. R. Naseh, "Novel Sliding Mode Control Approach for Quasi-Z-Source Converters with Improved Performance," *International Journal of Industrial Electronics Control and Optimization*, vol. 7, no. 3, pp. 213–224, 2024.

[14] A. Zakipour, S. Shokri Kojori, and M. Tavakoli Bina, "Closed-loop Control of the Grid-connected Z-source Inverter Using Hyper-plane MIMO Sliding Mode," *IET Power Electronics*, vol. 10, no. 15, pp. 2229–2241, 2017.

[15] Y. Zhang, C. Fu, M. Sumner, and P. Wang, "A Wide Input-Voltage Range Quasi-Z-Source Boost DC–DC Converter With High-Voltage Gain for Fuel Cell Vehicles," *IEEE Transactions on Industrial Electronics*, vol. 65, no. 6, pp. 5201–5212, 2018.

[16] J. R. Gazoli, M. G. Villalva, and E. Ruppert, "Micro-Inverter for Integrated Grid-Tie Photovoltaic Module Using Resonant Controller," *International Transactions on Electrical Energy Systems*, vol. 24, no. 5, pp. 713–722, 2013.

[17] M. Salimi, J. Soltani, G. A. Markadeh, and N. R. Abjadi, "Indirect Output Voltage Regulation of DC–DC Buck/Boost Converter Operating in Continuous and Discontinuous Conduction Modes Using Adaptive Backstepping Approach," *IET Power Electronics*, vol. 6, no. 4, pp. 732–741, 2013.

[18] Y. Tang, and S. Xie, "System Design of Series Z-source Inverter with Feedforward and Space Vector Pulse-width Modulation Control Strategy," *IET Power Electronics*, vol. 7, no. 3, pp. 736–744, 2014.

[19] Y. Li, S. Jiang, J. G. Cintron-Rivera, and F. Z. Peng, "Modeling and Control of Quasi-Z-Source Inverter for Distributed Generation Applications," *IEEE Transactions on Industrial Electronics*, vol. 60, no. 4, pp. 1532–1541, 2013.

[20] H. Rostami, and D. A. Khaburi, "Neural Networks Controlling for Both the DC Boost and AC Output Voltage of Z-Source Inverter," *2010 1st Power Electronic & Drive Systems & Technologies Conference (PEDSTC)*, pp. 135–140, 2010.

[21] P. Iniyaval, and S. R. Karthikeyan, "Fuzzy Logic Based Quasi Z-Source Cascaded Multilevel Inverter with Energy Storage for Photovoltaic Power Generation System," *2016 International Conference on Emerging Trends in Engineering, Technology and Science (ICETETS)*, pp. 1–5, 2016.

[22] A. Ayad, P. Karamanakos, and R. Kennel, "Direct Model Predictive Current Control Strategy of Quasi-Z-Source Inverters," *IEEE Transactions on Power Electronics*, vol. 32, no. 7, pp. 5786–5801, 2017.

[23] F. Bagheri, H. Komurcugil, O. Kukrer, N. Guler, and S. Bayhan, "Multi-Input Multi-Output-Based Sliding-Mode Controller for Single-Phase Quasi-Z-Source Inverters," *IEEE Transactions on Industrial Electronics*, vol. 67, no. 8, pp. 6439–6449, 2020.

[24] A. Zakipour, S. Shokri-Kojori, and M. Tavakoli Bina, "Sliding Mode Control of the Nonminimum Phase Grid-Connected Z-Source Inverter," *International Transactions on Electrical Energy Systems*, vol. 27, no. 11, e2398, 2017.

Declaration of competing interest

The authors declare that they have no known competing financial interests or personal relationships that could have appeared to influence the work reported in this paper. The ethical issues, including plagiarism, informed consent, misconduct, data fabrication and/or falsification, double publication and/or submission, redundancy, have been completely observed by the authors.

Bibliography



Gholamreza Shahabadi was born in Birjand in 1983. He obtained his MS degree from the Faculty of Engineering at Islamic Azad University, Gonabad branch, Iran, in 2008. Later, he pursued his PhD degree in Electrical Engineering at the Islamic Azad University, Birjand branch, Iran, in 2024. Since 2025, he has been working at the University of Skill, South Khorasan Branch, Iran. His research interests include DC–DC converter design and control, machine learning, audio signal processing, and hybrid electric vehicles.
Email: Ghr.shahabady@gmail.com
ORCID: 0000-0002-9333-2789
Contribution Statement: Conceptualization, Data curation, Formal analysis, Methodology, Software, Visualization, Roles/Writing - original draft, Writing-review & editing.



Siavash Es'haghi is an Assistant Professor at the Science and Research Campus, Islamic Azad University, Tehran, Iran. He received his B.Sc. in Electronics from Iran University of Science and Technology, Tehran, his M.Sc. in Electronics from Malek-Ashtar University of Technology, Tehran, and his Ph.D. in Electronics from Shahid Beheshti University, Tehran. His research interests include digital electronics, high-level synthesis, reliability, hardware accelerators, and hardware security.
Email: s_esshaghi@iau.ac.ir
ORCID: 0000-0003-1031-628X
Contribution Statement: Supervision, Validation, Writing-review & editing.



Javad Pourhossein received the B.S. degree in electrical engineering from Sharif University of Technology, Tehran, Iran, in 1992, the M.S. degree in electrical engineering from Islamic Azad University (IAU) - South Tehran Br., Tehran, in 1999 and the Ph.D. degree in electrical engineering from IAU- Science and Research Br., Tehran, in 2012. He is currently an Assistant Professor at IAU- Gonabad Br. His research interests are Flexible AC Transmission System devices, power system stability, optimization of electrical energy systems and renewable resources.
Email: Javad.Pourhossein@iau.ac.ir
ORCID: 0000-0002-8661-6011
Contribution Statement: Supervision, Validation, Writing-review & editing.